Saturation of thermoacoustic mixture separation

D. A. Geller and G. W. Swift
Condensed Matter and Thermal Physics Group, Los Alamos National Laboratory, Los Alamos, New Mexico 87545

(Received 19 January 2001; revised 27 November 2001; accepted 17 December 2001)

The theory for thermoacoustic mixture separation is extended to include the effects of a nonzero concentration gradient. New data are presented, which are in excellent agreement with this theory. The maximum concentration gradient which may be achieved in a binary mixture of gases through this separation process is intrinsically limited by the fractional pressure amplitude, by the tidal displacement, and by the size of the thermal diffusion ratio. Ordinary diffusion further detracts from the attainable final concentration gradient and can become the dominant remixing process as the cross section of the duct is increased. Rayleigh streaming also works against thermoacoustic separation, and an estimate of the molar flux from streaming is given. © *2002 Acoustical Society of America.* [DOI: 10.1121/1.1453449]

PACS numbers: 43.35.Ud, 43.20.Mv, 43.35.Ty [SGK]

I. INTRODUCTION

Recently, Swift and Spoor[1] (S&S) showed theoretically how the propagation of acoustic waves through a mixture of gases in a duct can cause the time-averaged separation of light and heavy molecules along the wave-propagation direction by means of processes occurring at the boundary layer. The separation is second order in the dynamical variables and can lead to large separation rates and concentration gradients. The strength of this separation mechanism depends both on the properties of the gas mixture and on the phasing of the acoustic field. Spoor and Swift[2] experimentally found that the separation saturates exponentially, and they were able to generate final concentration gradients as large as 7% per meter for 50–50 He–Ar starting mixtures in a tube of approximately 5 mm diameter. However, the focus of their attention was on the initial rate of separation, before significant concentration gradients had developed, because the theory of S&S was limited to that situation.

In this paper, we investigate the separation process in the presence of a nonzero concentration gradient in order to understand the saturation separation. Several processes work against the separation mechanism of S&S to determine the final gradient. Our most important new result is that the separation in a duct is intrinsically limited by the square of the amplitude of displacement of the gas in the acoustic wave. In addition, the remixing arising from concentration-gradient-driven mutual diffusion is typically a large effect. Although we do not study the effect thoroughly here, Rayleigh streaming may also contribute a substantial remixing flux, depending on the shape of the duct and on the intensity of the acoustic field.

In what follows, we first introduce and define the important physical and mathematical parameters in this problem. We then present a heuristic argument, assuming standing-wave phasing, for the intrinsic limitation of the separation process. In the next few sections we extend the S&S theory to lowest order in the concentration gradient and find the expression determining the saturation of the separation process. We conclude by describing our experiments supporting this more complete theory.

II. IMPORTANT QUANTITIES

Since early in the last century,[3] it has been understood that application of a thermal gradient to a binary mixture of gases can yield a gradient in the molar concentrations of the constituent gases. Ordinary mutual diffusion opposes this thermal diffusion process; and for a closed, isobaric volume of a mixture, the steady state is reached when

$$\nabla n_H = -k_T \nabla \ln T, \tag{1}$$

where n_H is, by convention, the mole fraction of the heavier of the two gases and k_T is called the thermal diffusion ratio. Frequently—but not always—thermal diffusion drives the heavier gas toward the lower temperature region, so these conventions normally lead to positive values for k_T. For He–Ar, the binary mixture used in our experiments, we use $k_T = 0.38\,(1-n_H)^{1.2} n_H^{0.8}$ based on a fit to the data of Atkins *et al.*[4]

Following S&S, our analysis is based on the notation of Landau and Lifshitz,[5] which accounts for the concentrations of gases by mass fraction instead of mole fraction. Hence, we define the heavy mass fraction c by

$$c = n_H m_H / m_{\text{avg}}, \tag{2}$$

where the molar-average mass m_{avg} can be expressed in either of two ways

$$m_{\text{avg}} = n_H m_H + (1-n_H) m_L, \tag{3}$$

$$m_{\text{avg}}^{-1} = c m_H^{-1} + (1-c) m_L^{-1}, \tag{4}$$

and m_L and m_H are the molar masses of the light and heavy gases, respectively. In order to write the mass flux density from diffusion in terms of c rather than n, we must use the scaled thermal diffusion ratio

$$k_T' = k_T m_L m_H / m_{\text{avg}}^2, \tag{5}$$

which is Eq. (44) in S&S, in place of k_T.

The effect in which we are interested occurs via acoustic processes within the thermal and viscous boundary layers. To study this analytically, we consider the gas in an acoustic duct, with sound of a single frequency f propagating along the axis of the duct. The wavelength $\lambda = a/f$, where a is the speed of sound in the gas mixture, is taken to be much larger than all other length scales in the system, including the transverse dimensions of the duct characterized by r_h, the hydraulic radius.[6] The thermoacoustic variables can be expanded in harmonics to first order

$$\begin{aligned} p &= p_m + \Re[p_1(x)e^{\imath\omega t}], \\ T &= T_m + \Re[T_1(x,r)e^{\imath\omega t}], \\ \rho &= \rho_m(x) + \Re[\rho_1(x,r)e^{\imath\omega t}], \\ u &= \Re[u_1(x,r)e^{\imath\omega t}], \\ c &= c_m(x) + \Re[c_1(x,r)e^{\imath\omega t}], \end{aligned} \tag{6}$$

where $\omega = 2\pi f$ is the angular frequency of the acoustic field and x is the longitudinal coordinate along the acoustic duct. The parameter r stands for the radial coordinate if the duct is a circular tube, for the coordinate y normal to the duct's wall in the boundary-layer approximation, or for both coordinates perpendicular to x in ducts of lower symmetry. Symbols p, T, ρ, u, and c are the pressure, temperature, mass density, x component of velocity, and concentration of the heavy component, respectively. The thickness of the thermal boundary layer is the thermal penetration depth

$$\delta_\kappa = \sqrt{2k/\omega\rho c_p} = \sqrt{2\kappa/\omega}, \tag{7}$$

where k is the thermal conductivity of the gas, c_p is the isobaric heat capacity per unit mass, and κ is the thermal diffusivity. Similarly, the viscous boundary layer is defined by the viscous penetration depth

$$\delta_\nu = \sqrt{2\mu/\omega\rho} = \sqrt{2\nu/\omega}, \tag{8}$$

where μ is the viscosity and ν is the kinematic viscosity. Another fundamental length scale involved in the mixture system is the mass diffusion length

$$\delta_D = \sqrt{2D/\omega}, \tag{9}$$

where $D = D_{12}$ is the mutual diffusion coefficient for the binary mixture.

It is convenient to define two ratios of the length scales that appear repeatedly in the analysis. The Prandtl number is defined as

$$\sigma = (\delta_\nu/\delta_\kappa)^2, \tag{10}$$

and describes the relative extent of the viscous and thermal effects. This ratio is $\leqslant 2/3$ for binary mixtures of monatomic ideal gases. A second ratio is

$$L = (\delta_\kappa/\delta_D)^2, \tag{11}$$

which compares the relative importance of thermal conduction to mass diffusion.

III. A SIMPLE BUCKET-BRIGADE MODEL

S&S showed that the time-averaged separation flux along x is due to oscillating motion and concentration, with suitable time phasing, in the gas about a thermal penetration depth from the wall of the duct. These phased oscillations constitute a bucket-brigade shuttling of one component in the x direction and the other component in the $-x$ direction. In order to depict this process it was useful to consider the behavior of the gas at a fixed location in a duct, but for describing saturation qualitatively in this section it is easier to follow the processes in moving parcels of the gas. To gain intuition about the most interesting mechanism that causes saturation of the time-averaged concentration gradient in the duct, we consider the caricature of oscillations with standing-wave phasing shown in Fig. 1.

In this crude approximation, the time-averaged separation flux may be carried by the gas parcel approximately δ_κ from the wall, because this parcel may experience both oscillating concentration and oscillating motion (with suitable phasing). Hence, the time-averaged separation flux will stop when the concentration oscillation $|c_1|$ is zero in the gas parcel approximately δ_κ from the wall. This will occur when the oscillating diffusion between that parcel and those adjacent to the wall, indicated by the wide arrows, is also zero.

According to Eq. (58.11) from Landau and Lifshitz,[5] the diffusive mass-flux density vector is

$$\mathbf{i} = -\rho D\left[\nabla c + \frac{k_T'}{T}\nabla T\right]. \tag{12}$$

Using Fig. 1 to estimate the values on the right-hand side of Eq. (12) when the transverse component of the flux $i_y = 0$, and hence $|c_1| = 0$, for the parcel a distance δ_κ from the wall yields

$$0 = \frac{c_m - (c_m + |x_1|\, dc_m/dx)}{\delta_\kappa} + \frac{k_T'}{T_m}\frac{|T_1|}{\delta_\kappa}, \tag{13}$$

so that

$$\left(\frac{dc_m}{dx}\right)_{\text{sat}} \sim \frac{k_T'}{T_m}\frac{|T_1|}{|x_1|}. \tag{14}$$

Finally, using $T_1 = p_1/\rho_m c_p$ and $x_1 = \langle u_1\rangle/\imath\omega$, where $\langle\ \rangle$ denotes the spatial average over the duct's cross section, this becomes[7]

$$\left(\frac{dc_m}{dx}\right)_{\text{sat}} \sim \frac{\gamma-1}{\gamma}k_T'\frac{|p_1|}{p_m}\frac{\omega}{|\langle u_1\rangle|}. \tag{15}$$

We can expect that the quantitative theory developed in the next sections will be in qualitative agreement with Eq. (15), so that the thermoacoustic mixture separation can only occur when the concentration gradient is less than approximately $(dc_m/dx)_{\text{sat}}$. For future convenience, then, let us define $(dc_m/dx)_{\text{sat}}$ exactly according to Eq. (15), and we also define

$$\Gamma_c = \frac{dc_m/dx}{(dc_m/dx)_{\text{sat}}}. \tag{16}$$

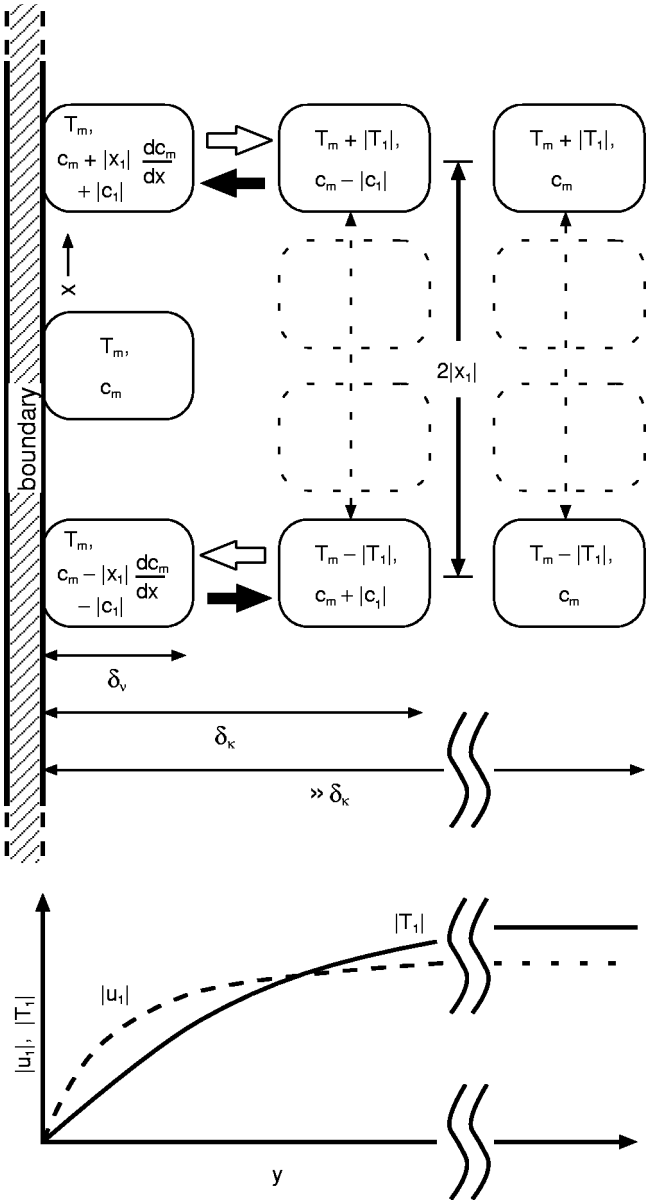

FIG. 1. Illustration of five typical parcels of gas, to guide the intuition about the saturation concentration difference. The three parcels abutting the wall are immobilized by viscosity. The parcel farthest from the wall, shown at the two extremes of its motion, is too far from the wall to experience oscillating temperature gradients or oscillating concentrations. The intervening parcel, also shown at the two extremes of its motion, *might* experience concentration oscillations $|c_1|$ due to oscillating thermal diffusion, indicated by the wide arrows. The filled wide arrows represent diffusion of the heavy component, while the open arrows represent diffusion of the light component. The thermal diffusion ratio k_T is assumed to be positive, as for the He–Ar mixtures in our experiments. The heavy component diffuses toward the isothermal boundary during compression, provided that the longitudinal concentration gradient dc_m/dx is not too large. In this boundary-layer picture, we denote the transverse coordinate by y in place of r.

Γ_c is always real and may loosely be regarded as a figure of merit for the progress of the separation process toward saturation.[8]

IV. THE FIRST-ORDER THEORY

We can derive the lowest-order theory for the saturation of thermoacoustic separation by preserving terms containing the longitudinal concentration gradient dc_m/dx in the equations of two-component fluid dynamics. We will continue to assume $dT_m/dx=0$ as in S&S, because our result will be complicated enough even in the absence of a temperature gradient.

From S&S Eqs. (17)–(18) for the convection and diffusion of c,

$$\frac{\partial c}{\partial t}+\mathbf{u}\cdot\nabla c=-\frac{1}{\rho}\nabla\cdot\mathbf{i}=\nabla\cdot\left[D\nabla c+\left(\frac{Dk_T'}{T}\right)\nabla T\right], \tag{17}$$

we now obtain

$$c_1+\frac{u_1}{\imath\omega}\frac{dc_m}{dx}=\frac{\delta_D^2}{2\imath}\left[\nabla_r^2 c_1+\frac{k_T'}{T_m}\nabla_r^2 T_1\right], \tag{18}$$

to first order in the oscillating quantities, where ∇_r^2 denotes the parts of the Laplacian belonging to the transverse coordinates.

We now write Eq. (20) from S&S for the first-order oscillating heat transfer (or diffusion of entropy) in the gas mixture

$$\rho_m T_m\left(\imath\omega s_1+u_1\frac{ds_m}{dx}\right)$$
$$=k\nabla_r^2 T_1-\left[k_T'\left(\frac{\partial g}{\partial c}\right)_{p,T}-T_m\left(\frac{\partial g}{\partial T}\right)_{p,c}\right]\nabla\cdot\mathbf{i}_1, \tag{19}$$

where g is the Gibbs free energy per unit mass, and with the divergence of the first-order oscillating mass flux

$$\nabla\cdot\mathbf{i}_1=-\imath\omega\rho_m c_1-\rho_m u_1\frac{dc_m}{dx}, \tag{20}$$

according to Eqs. (17) and (18) above. We cannot discard the ds_m/dx term, as the gradient in entropy will not be negligible when there is a concentration gradient along the duct. Instead, we use the identity (22) from S&S to write

$$\frac{ds_m}{dx}=\frac{c_p}{T_m}\frac{dT_m}{dx}-\left(\frac{\partial g}{\partial T}\right)_{p,c}\frac{dc_m}{dx}-\frac{1}{\rho_m T_m}\frac{dp_m}{dx}. \tag{21}$$

The first term on the right-hand side is zero, because of our assumption at the outset of zero temperature gradient. The last term is zero too, because we assume that the mean pressure is constant throughout the duct. If we eliminate s_1 from (19) by means of S&S's (22), substitute our (21) into (19), and define for future convenience the dimensionless quantity

$$\varepsilon\equiv\frac{(k_T')^2}{c_p T_m}\left(\frac{\partial g}{\partial c}\right)_{p,T}=\frac{\gamma-1}{\gamma}\frac{k_T^2}{n_H(1-n_H)}, \tag{22}$$

as in S&S Eqs. (24) and (45), we finally obtain

$$T_1=\frac{p_1}{\rho_m c_p}+\frac{\varepsilon T_m}{k_T'}c_1+\frac{\delta_\kappa^2}{2\imath}\nabla_r^2 T_1+\frac{\varepsilon T_m}{\imath\omega k_T'}\frac{dc_m}{dx}u_1. \tag{23}$$

This differential equation differs from (23) of S&S only through the appearance of the new, final term on the right.

Up to this point we have avoided specifying our duct geometry, and we can proceed a bit further in that mode. First, note that we can write u_1 in terms of its average over the cross-sectional area $\langle u_1\rangle$ as

$$u_1 = \frac{\langle u_1 \rangle}{1-f_\nu}(1-h_\nu), \tag{24}$$

where $(1-h_\nu)$ describes the velocity profile as a function of position on the cross section, and $f_\nu \equiv \langle h_\nu \rangle$. Equations (18) and (23) constitute two coupled partial differential equations in T_1 and c_1. Solving Eq. (23) for c_1, inserting the result in (18), and using Eq. (24) yields

$$T_1 = \frac{p_1}{\rho_m c_p} + \frac{1}{2\imath}[\delta_\kappa^2 + \delta_D^2(1+\varepsilon)]\nabla_r^2 T_1 + \frac{\delta_\kappa^2 \delta_D^2}{4}\nabla_r^4 T_1 + \frac{\delta_D^2}{2\imath}\frac{\langle u_1 \rangle}{1-f_\nu}\frac{\varepsilon T_m}{\imath \omega k_T'}\frac{dc_m}{dx}\nabla_r^2 h_\nu, \tag{25}$$

which is similar to Eq. (27) of S&S. This can now be solved for T_1 as a function of the coordinates. Because of the new term appearing on the right, this inhomogeneous differential equation for T_1 is driven by the concentration gradient and u_1, as well as by p_1.

To determine a solution for T_1, we must apply appropriate boundary conditions to our fourth-order differential equation. One boundary condition is provided by assuming the wall of the duct to be isothermal, so that $T_1 = 0$ at the wall. The wall is generally isothermal because the solid has a much higher heat capacity and thermal conductivity than the gas. A second boundary condition can be taken by requiring that there be no net flux of concentration into the wall

$$i_r|_{\text{wall}} \propto \left[\nabla_r c_1 + \frac{k_T'}{T_m}\nabla_r T_1\right]_{\text{wall}} = 0. \tag{26}$$

Inserting (23) and (24), this becomes

$$0 = \left[(1+\varepsilon)\nabla_r T_1 - \frac{\delta_\kappa^2}{2\imath}\nabla_r^3 T_1 + \frac{\langle u_1 \rangle}{1-f_\nu}\frac{\varepsilon T_m}{\imath \omega k_T'}\frac{dc_m}{dx}\nabla_r h_\nu\right]_{\text{wall}}. \tag{27}$$

For some duct geometries, such as the infinite slab, these two boundary conditions specify four equations, so that the solution is uniquely defined. For the boundary-layer and circular-tube geometries we consider, though, these conditions provide only two equations and it is necessary to impose the additional restriction that the solution be finite everywhere inside the duct.

To proceed further, one must now specify a geometry for the duct. The boundary-layer solution is of limited practical interest, but it yields a relatively simple expression for the separation flux and demonstrates the main features of thermoacoustic separation which are present in any geometry. In the boundary-layer limit (transverse duct dimensions $\gg \delta_\nu$), we have $\nabla_r^2 \equiv \partial^2/\partial y^2$, with y the direction perpendicular to the boundary. We will also investigate the problem for a circular tube of arbitrary diameter: the algebraic manipulations are almost identical, except for the presence of some normalization factors that prevent simplifications from occurring. In the circular tube, $\nabla_r \to \partial/\partial r$ and $\nabla_r^2 \to (1/r)\partial/\partial r(r\ \partial/\partial r)$, and we ignore the ϕ derivatives because of cylindrical symmetry.[9] In Eqs. (25) and (27), we also interpret the higher-order differential operators as $\nabla_r^3 \to \nabla_r \nabla_r^2$ and $\nabla_r^4 \to \nabla_r^2 \nabla_r^2$, consistent with the derivation of these equations.

For the boundary-layer limit

$$h_\nu = e^{-(1+\imath)y/\delta_\nu} \quad \text{and} \quad f_\nu = \frac{(1-\imath)\delta_\nu}{2r_h}, \tag{28}$$

while for a circular tube of radius R, the oscillating velocity u_1 of Eq. (24) is expressed in terms of

$$h_\nu = \frac{J_0[(\imath-1)r/\delta_\nu]}{J_0[(\imath-1)R/\delta_\nu]}, \qquad f_\nu = \frac{2\,J_1[(\imath-1)R/\delta_\nu]}{J_0[(\imath-1)R/\delta_\nu](\imath-1)R/\delta_\nu}, \tag{29}$$

where the J_i are cylindrical Bessel functions. Direct substitution shows that the solution to Eq. (25) must be of the form

$$T_1 = \frac{p_1}{\rho_m c_p}[1 - B\,h_\nu - C\,h_{\kappa D} - (1-B-C)h_{D\kappa}], \tag{30}$$

with the same length scales for the y or r dependence as found by S&S

$$\delta_{\kappa D}^2 = \tfrac{1}{2}\delta_\kappa^2[\,1 + (1+\varepsilon)/L + \sqrt{[1+(1+\varepsilon)/L]^2 - 4/L}\,], \tag{31}$$

$$\delta_{D\kappa}^2 = \tfrac{1}{2}\delta_\kappa^2[\,1 + (1+\varepsilon)/L - \sqrt{[1+(1+\varepsilon)/L]^2 - 4/L}\,]. \tag{32}$$

For the boundary-layer calculation, we choose all the δs to be positive, in order to satisfy the aforementioned requirement that the solution remain finite as $y \to \infty$. For the cylindrical tube, we can choose the δs to be positive because the functions J_0 are even; the Y_0 solutions to Eq. (25) have been discarded because they diverge at the center of the tube. The final coefficient $1-B-C$ in Eq. (30) has been chosen so that the isothermal boundary condition, $T_1|_{\text{wall}} = 0$, is explicitly obeyed. Substitution into Eq. (25) leads to

$$B = \frac{\imath e^{-\imath\theta}\varepsilon}{1-f_\nu}\frac{\sigma}{(1-\sigma)(1-\sigma L) - \varepsilon\sigma}\Gamma_c, \tag{33}$$

where θ is the phase of the acoustic impedance, i.e., the phase by which p_1 leads U_1. Next, substitution into the unusual ''zero transverse flux'' boundary condition (27) yields

$$C = \frac{f_{D\kappa}(\delta_\kappa^2/\delta_{D\kappa}^2 - 1) - B[f_\nu(\sigma-1)/\sigma + f_{D\kappa}(\delta_\kappa^2/\delta_{D\kappa}^2 - 1)]}{f_{D\kappa}(\delta_\kappa^2/\delta_{D\kappa}^2 - 1) - f_{\kappa D}(\delta_\kappa^2/\delta_{\kappa D}^2 - 1)}. \tag{34}$$

In the boundary-layer approximation, this simplifies further to

$$C_{\text{BL}} = C_{\text{S\&S}}\left[1 - B\left(1 + \frac{\sigma-1}{\sqrt{\sigma}}\frac{\delta_\kappa}{\sqrt{L}\,\delta_{\kappa D} - \delta_{D\kappa}}\right)\right], \tag{35}$$

where $C_{\text{S\&S}}$ is defined as in Eq. (33) of S&S

$$C_{\text{S\&S}} = \frac{\sqrt{L}\,\delta_{\kappa D} - \delta_{D\kappa}}{(1+\sqrt{L})(\delta_{\kappa D} - \delta_{D\kappa})}. \tag{36}$$

One sees immediately that for $dc_m/dx \to 0$,

$$B \to 0 \quad \text{and} \quad C_{\mathrm{BL}} \to C_{\mathrm{S\&S}}. \tag{37}$$

So, our expression returns the results of S&S when the concentration gradient is zero. Whether or not the concentration gradient is zero, Eq. (30) for the complex temperature T_1 reduces to the ordinary thermoacoustic result as the thermal diffusion ratio is reduced to zero, just like the expression (30) of S&S. When $k_T' \to 0$ and, therefore, $\varepsilon \to 0$, it follows that $B \to 0$; and, as before (i) if $L \geqslant 1$, then $\delta_{\kappa D} \to \delta_\kappa$, $\delta_{D\kappa} \to \delta_D$, and $C \to 1$, and (ii) if $L < 1$, then $\delta_{\kappa D} \to \delta_D$, $\delta_{D\kappa} \to \delta_\kappa$, and $C \to 0$.

Finally, the complex concentration c_1 can be determined by inserting Eq. (30) for T_1 into Eq. (23), with (24) and either (28) or (29)

$$c_1 = -\frac{p_1}{\rho_m c_p}\frac{k_T'}{\varepsilon T_m}\left[C\left(1-\frac{\delta_\kappa^2}{\delta_{\kappa D}^2}\right)h_{\kappa D} + (1-B-C)\left(1-\frac{\delta_\kappa^2}{\delta_{D\kappa}^2}\right)h_{D\kappa} + B\left(1-\frac{1}{\sigma}\right)h_\nu + \frac{\rho_m c_p}{p_1}\frac{\langle u_1\rangle}{1-f_\nu}\frac{\varepsilon T_m}{\imath\omega k_T'}\frac{dc_m}{dx}(1-h_\nu)\right]. \tag{38}$$

Notice in particular the fourth term in this equation, which is proportional to $(-u_1/\imath\omega)\cdot dc_m/dx = -x_1 \cdot dc_m/dx$ where x_1 denotes the complex first-order oscillating particle displacement (i.e., the tidal displacement). In other words, this term describes the change in concentration inside a stationary control volume due to the flow of gas into this volume from a point about x_1 away along the axis of the tube, where the mean concentration will generally be different when $dc_m/dx \neq 0$. This portion of the oscillating local concentration, call it c_{x1}, becomes comparable to the other terms as the concentration gradient approaches its saturation value. However, c_{x1} does not ultimately contribute to the time-averaged transport of concentration, because it is exactly 90° out of phase from the conjugate velocity $\tilde{u}_1$.

V. THE SEPARATION FLUX THROUGH SECOND ORDER

Next, we seek the time-averaged mole flux of the heavy component along the x axis, through second order. From Landau and Lifshitz,[5] the mass-flux densities are $\rho c u + i$ and $\rho(1-c)u - i$ for the heavy and light components, respectively; this is necessary in order to preserve the definition of u as equal to the momentum of a unit mass of the gas. The mole fluxes of the two components are therefore

$$\dot{N}_H = A\langle \overline{\rho c u} + \overline{i}\rangle / m_H, \tag{39}$$

and

$$\dot{N}_L = A\langle \overline{\rho(1-c)u} - \overline{i}\rangle / m_L, \tag{40}$$

where i is the x component of $\mathbf{i}$ and the overbar denotes the time average. For the equimolar process of interest to us, $\dot{N}_H = -\dot{N}_L$. Expanding Eq. (39) yields

$$\dot{N}_H = \dot{N}_{H,m} + \dot{N}_{H,2} + \dot{N}_{H,4} + \cdots, \tag{41}$$

where the odd-order terms are zero because the time average of a periodic function is zero.

Setting $\dot{N}_{H,m} = -\dot{N}_{L,m}$ yields a mean velocity

$$u_m = \frac{m_{\mathrm{avg}}(m_H - m_L)}{m_H m_L}\frac{i_m}{\rho_m}. \tag{42}$$

Formally, this should have been included in Eq. (6), but we argue here that it is negligible. There are three ways in which u_m could potentially modify the results of acoustics as derived here. The first-order continuity equation (18) would, in principle, gain a term $(u_m/\imath\omega)dc_1/dx$, but this contribution is of order δ_D/λ smaller than all the other terms in that approximate equation and can be ignored, as long as λ is much larger than any other length scale in the system. The equation for heat transfer (19) would also gain a new first-order term $\rho_m T_m u_m (ds_1/dx)$, but this contribution is again of order δ_D/λ smaller than the other terms in that equation. Finally, in our expression below for the second-order mole flux (45) there would emerge a new term $(A/2)u_m \Re[\langle \tilde{\rho}_1 c_1\rangle]$, but this portion of the flux is approximately u_m/a times smaller than the main term $(A/2)\rho_m \Re[\langle c_1 \tilde{u}_1\rangle]$. In our experiments, we always had $u_m/a < 5\times 10^{-8}$ so that the $u_m\langle\tilde{\rho}_1 c_1\rangle$ contribution to the flux was negligible. We thus can safely ignore this u_m from steady diffusion, a mean flow which the experimenter does not directly adjust, in our harmonic expansion of the velocity $u(x,r)$ in Eq. (6). Further, we note that the arguments above hold identically for an externally imposed steady flow velocity u_m. In that case, an arbitrary u_m will not affect the mole fluxes associated with the acoustics, provided that $u_m \ll a$. Only the zeroth-order mole fluxes Eqs. (39) and (40) will change through the addition of this imposed u_m to the mean velocity from Eq. (42), and the mole fluxes measured in a frame moving with velocity u_m are the same as the mole fluxes when the applied $u_m = 0$.

Using Eqs. (42) and (12) (with $dT_m/dx = 0$) in Eq. (39) yields

$$\dot{N}_{H,m} = -\rho A D \frac{dc_m}{dx}\frac{m_{\mathrm{avg}}}{m_L m_H} \tag{43}$$

for the zeroth-order diffusive molar flux of the heavy component. Using Eqs. (2) and (3), this can be recast in the more familiar form

$$\dot{N}_{H,m} = -NAD\frac{dn_H}{dx}, \tag{44}$$

where N is the total number of moles per unit volume. Unlike the thermal diffusion ratio k_T [cf. Eq. (5)], the diffusion constant D is the same for either measure of concentration, n_H or c. This ordinary diffusion, driven by the concentration gradient along x but independent of the acoustic field, always works against the molar flux of thermoacoustic mixture separation derived next.

Using Eq. (39) to write all possible second-order terms for $\dot{N}_{H,2}$ yields a sum of many terms, each of which can have factors with subscripts m, 1, and 2. The terms containing u_m are negligible at this order, as argued above. The i_2 term,

proportional to Ddc_2/dx, is negligible compared to $\dot{N}_{H,m}$ for the non-negligible dc_m/dx of interest to us. This leaves us with simply

$$\dot{N}_{H,2}=\frac{A\rho_m}{2m_H}\Re[\langle c_1\tilde{u}_1\rangle]+\frac{c_m}{m_H}\dot{M}_2, \tag{45}$$

where $\dot{M}_2=A\ \Re[\langle\rho_1\tilde{u}_1\rangle]/2+A\rho_m\langle u_{2,0}\rangle$ is the net second-order mass flux, and A is the cross-sectional area of the duct. Using $\dot{N}_H=-\dot{N}_L$ again, this time at second order, and again neglecting i_2 gives

$$\dot{M}_2=\dot{M}_{H,2}(1-m_L/m_H). \tag{46}$$

Combining Eqs. (45) and (46), we finally have for the second-order mole flux of the heavier component

$$\dot{N}_{H,2}=\frac{m_{\text{avg}}}{m_Hm_L}\frac{A\rho_m}{2}\Re[\langle c_1\tilde{u}_1\rangle]. \tag{47}$$

Using Eqs. (38) and (24), along with the definition of volumetric velocity $U_1=A\langle u_1\rangle$, we can write

$$\begin{aligned}\frac{A\rho_m}{2}\Re[\langle c_1\tilde{u}_1\rangle]&=\frac{1}{2}\frac{k_T'/\varepsilon}{c_pT_m}\Re\left\{\frac{p_1\tilde{U}_1}{1-\tilde{f}_\nu}\left[C\left(\frac{\delta_\kappa^2}{\delta_{\kappa D}^2}-1\right)\langle h_{\kappa D}(1-\tilde{h}_\nu)\rangle\right.\right.\\&+(1-B-C)\left(\frac{\delta_\kappa^2}{\delta_{D\kappa}^2}-1\right)\langle h_{D\kappa}(1-\tilde{h}_\nu)\rangle\\&\left.\left.+B\frac{\sigma-1}{\sigma}\langle h_\nu(1-\tilde{h}_\nu)\rangle\right]\right\}.\end{aligned} \tag{48}$$

The thermoacoustic mole flux from Eqs. (47) and (48), plus the mole flux from diffusion given above in Eq. (44), was integrated using the Bessel-function forms for the h_i, and is compared with the data in Sec. VII.

Further progress can be made in the boundary-layer approximation. Making use of the integral identity (47) from S&S, we calculate

$$\begin{aligned}\frac{A\rho_m}{2}\Re[\langle c_1\tilde{u}_1\rangle]&=\frac{\delta_\kappa}{4r_h}\frac{k_T'/\varepsilon}{c_pT_m}\Re\left\{\frac{p_1\tilde{U}_1}{1-\tilde{f}_\nu}\left[C_{\text{BL}}\left(1-\frac{\delta_{\kappa D}^2}{\delta_\kappa^2}\right)\frac{(\delta_{\kappa D}/\delta_\kappa-\sqrt{\sigma})-\imath(\delta_{\kappa D}/\delta_\kappa+\sqrt{\sigma})}{(\delta_{\kappa D}^2/\delta_\kappa^2+\sigma)}\right.\right.\\&\left.\left.+(1-B-C_{\text{BL}})\left(1-\frac{\delta_{D\kappa}^2}{\delta_\kappa^2}\right)\frac{(\delta_{D\kappa}/\delta_\kappa-\sqrt{\sigma})-\imath(\delta_{D\kappa}/\delta_\kappa+\sqrt{\sigma})}{(\delta_{D\kappa}^2/\delta_\kappa^2+\sigma)}-B\frac{1}{\imath}\left(\frac{\sigma-1}{\sqrt{\sigma}}\right)\right]\right\}\end{aligned} \tag{49}$$

in place of S&S's intermediate result (48). If we take $r_h\gg\delta_\kappa$, this portion of the mass flux can again be coerced into a compact form similar to S&S's (49) to first order in δ/r_h

$$\begin{aligned}\frac{A\rho_m}{2}\Re[\langle c_1\tilde{u}_1\rangle]&=\frac{\delta_\kappa}{4r_h}\frac{k_T'}{c_pT_m}\{F_{\text{trav}}\Re[p_1\tilde{U}_1]\\&+F_{\text{stand}}\Im[p_1\tilde{U}_1]+F_{\text{grad}}|p_1||U_1|\Gamma_c\},\end{aligned} \tag{50}$$

where

$$F_{\text{trav}}=\frac{\sigma\sqrt{\sigma L}-\sqrt{\sigma}-\sigma\sqrt{L}(\delta_{\kappa D}/\delta_\kappa+\delta_{D\kappa}/\delta_\kappa)}{(1+\sqrt{L})[(1+\sigma)(1+\sigma L)+\varepsilon\sigma]}, \tag{51}$$

$$F_{\text{stand}}=\frac{-\sigma\sqrt{\sigma L}+\sqrt{\sigma}-\sigma\sqrt{L}(\delta_{\kappa D}/\delta_\kappa+\delta_{D\kappa}/\delta_\kappa)}{(1+\sqrt{L})[(1+\sigma)(1+\sigma L)+\varepsilon\sigma]}, \tag{52}$$

as before, and we additionally define

$$F_{\text{grad}}=\frac{\sqrt{\sigma}L(1-\sigma^2)(1+\sqrt{L})+\varepsilon\sqrt{\sigma}(\sqrt{L}-1)+[(\sigma^2-1)L+\varepsilon\sigma\sqrt{L}](\delta_{\kappa D}/\delta_\kappa+\delta_{D\kappa}/\delta_\kappa)}{(1+\sqrt{L})[(1+\sigma)(1+\sigma L)+\varepsilon\sigma][(1-\sigma)(1-\sigma L)-\varepsilon\sigma]/\sigma}, \tag{53}$$

representing the effect of the building gradient. We finally arrive at

$$\begin{aligned}\dot{N}_{H,2}&=\frac{\delta_\kappa}{4r_h}\frac{\gamma-1}{\gamma}\frac{k_T}{R_{\text{univ}}T_m}|p_1||U_1|\\&\times[F_{\text{trav}}\cos\theta+F_{\text{stand}}\sin\theta+F_{\text{grad}}\Gamma_c]\end{aligned} \tag{54}$$

in the boundary-layer limit, where R_{univ} is the universal gas constant. S&S plotted k_TF_{trav} and k_TF_{stand} vs mole fraction n_H for He–Ar mixtures; in Fig. 2 we reproduce those two curves and include the corresponding k_TF_{grad}, which is of comparable magnitude and also goes to zero at $n_H=0$ and $n_H=1$. Equation (54) shows that, neglecting $\dot{N}_{H,m}$, saturation of the separation process (i.e., $\dot{N}_{H,2}=0$) occurs at

$$\Gamma_c=-\frac{F_{\text{trav}}\cos\theta+F_{\text{stand}}\sin\theta}{F_{\text{grad}}}, \tag{55}$$

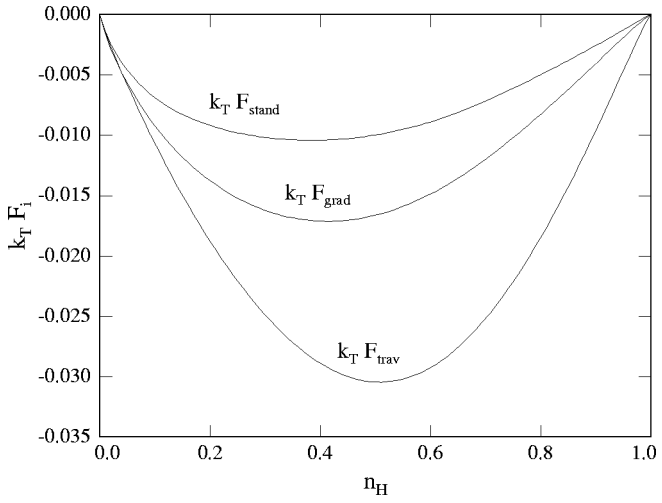

FIG. 2. Comparison of the three geometrical prefactors describing the separation flux for He–Ar.

which is of order 1 as we came to expect at the end of Sec. III, with details shown in Fig. 3.

Simply by substituting in the definition (16) for Γ_c, Eq. (54) can also be written as

$$\dot{N}_{H,2}=\frac{\delta_\kappa}{4r_h}\frac{\gamma-1}{\gamma}\frac{k_T}{R_{\mathrm{univ}}T_m}|p_1||U_1|[F_{\mathrm{trav}}\cos\theta+F_{\mathrm{stand}}\sin\theta]+\frac{\delta_\kappa}{4r_h}\frac{\rho_m|U_1|^2}{m_{\mathrm{avg}}\omega A}F_{\mathrm{grad}}\frac{dn_H}{dx}. \quad (56)$$

In this form, it is apparent that the new effect always opposes mixture separation, because $F_{\mathrm{grad}}<0$, and hence this term's contribution to $\dot{N}_{H,2}$ always opposes dn_H/dx. Being independent of p_1, this term represents a mixing phenomenon occurring in any laminar oscillating flow of a mixture in a duct. Watson[10] studied this problem in great detail, giving results for arbitrary r_h/δ_ν in circular and two-dimensional ''slab'' ducts. In our notation, Watson's boundary-layer result is

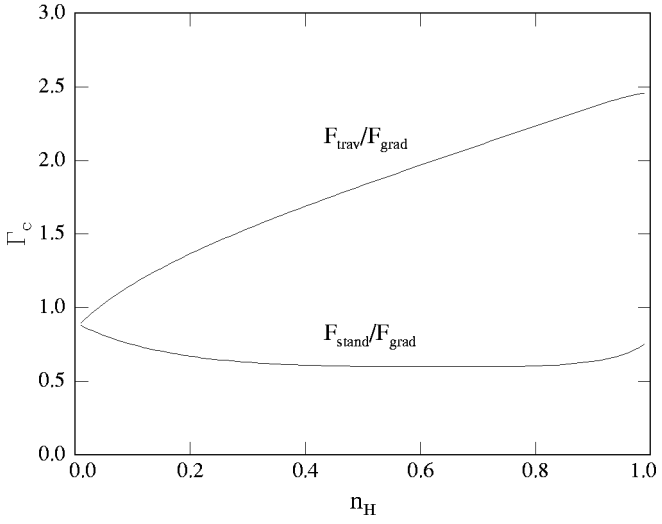

FIG. 3. The figure of merit for separation Γ_c for $\dot{N}_{H,2}=0$, as a function of Ar mole fraction in He–Ar mixtures for $\theta=180°$ and $\theta=270°$.

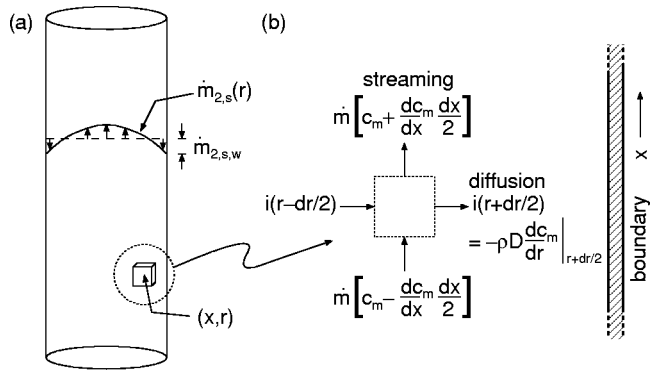

FIG. 4. (a) For laminar flow, the streaming mass-flux density is parabolic in the tube, except within the viscous boundary layer (negligibly thin in this figure), where it must approach zero at the wall. For a duct closed on both ends, the mass-flux density $\dot{m}_{2,s}(r)$ averages to zero over the cross section. (b) In the steady state, the net streaming flux of the heavy component into a fixed volume in space, centered on coordinates (x,r), is balanced by the flux of heavy mass out of this volume by diffusion.

$$\dot{N}_{H,2}=-\frac{\delta_\nu}{4r_h}\frac{\rho_m|U_1|^2}{m_{\mathrm{avg}}\omega A}\frac{\sqrt{\sigma L}}{(1+\sqrt{\sigma L})(1+\sigma L)}\frac{dn_H}{dx}. \quad (57)$$

This is identical to the $|U_1|^2$ term in Eq. (56), if our F_{grad} is evaluated with $\varepsilon=0$. Although ε is often small, Watson's neglect of it is not strictly valid. Mass diffusion and heat flux are inextricably linked in mixtures, as is most easily seen in our Eq. (23) with $p_1=0$, and so oscillating temperature should not necessarily be neglected in the problem Watson considered.

VI. REMIXING BY RAYLEIGH STREAMING

Rayleigh streaming[11] provides another mixing process that can work against thermoacoustic mixture separation. The steady circulation of Rayleigh streaming within the duct will tend to carry heavy-enriched gas in one direction in one part of the duct's cross section and light-enriched gas in the other direction in another part of the duct's cross section, as illustrated in Fig. 4, thereby mixing the separated gases. Fortunately, lateral diffusion of mass between these counterflowing streams will tend to reduce the net mixing, and will be most effective at doing so in small ducts.

We have found no citations in the literature regarding Rayleigh streaming in a gas mixture, including the effect of nonzero ε on T_1, and indeed this calculation appears very challenging. Hence, here we will provide only an order-of-magnitude estimate in boundary-layer approximation, in a circular tube, to get a rough idea of the magnitude of this effect and its dependence on key variables. The order of magnitude[11] of the second-order, streaming mass-flux density $\dot{m}_{2,s,w}$ just outside the boundary layer at the wall of the tube is

$$\dot{m}_{2,s,w}\sim|p_1||\langle u_1\rangle|/a^2. \quad (58)$$

This mass-flux density typically has a periodic dependence on the phase between p_1 and $\langle u_1\rangle$, and hence will be zero for some phasing, but we ignore this issue here. For laminar flow, the mass-flux-density distribution over most of the tube is then given by

$$\dot{m}_{2,s}(r)=\dot{m}_{2,s,w}(2r^2/R^2-1), \tag{59}$$

if we ignore the complicated details of how $\dot{m}_{2,s}$ goes to zero from the edge of the boundary layer to the wall itself and insist that $\langle \dot{m}_{2,s}\rangle=0$ for our closed system. This distribution of mass-flux density will tend to carry gas enriched in one component in one direction in the center of the tube, where $r<R/\sqrt{2}$, and gas enriched in the other component in the other direction in the rest of the tube.

In the absence of mitigating factors, these two counterflowing enriched-gas streams could be imagined as flowing independently along the entire length of the tube, effectively carrying light-enriched gas all the way from the ''light'' reservoir at one end of the tube to the ''heavy'' reservoir at the other end of the tube, and vice versa. Such mixing might be catastrophically large. Fortunately, for the experimental conditions of interest to us here, these two counterflowing streams have plenty of time to exchange significant mass with each other via diffusion, very analogous to the way heat is exchanged between fluid streams in a counterflow heat exchanger, so the remixing effect is greatly reduced. The characteristic transit time for streaming the full length l of the tube, $\rho_m l/\dot{m}_{2,s,w}$, is 10 to 100 times larger than the lateral diffusion time R^2/D. For a quantitative estimate of the magnitude of the mixing under these conditions, we consider the steady-state concentration $c_m(x,r)$ in a control volume at some fixed location (x,r) in the tube. The steady-state concentration is maintained by the competition between axial streaming flow along the concentration gradient and radial diffusion, obeying the equation

$$\dot{m}_{2,s}(r)\frac{dc_m(x,r)}{dx}=\rho_m D\frac{1}{r}\frac{d}{dr}r\frac{dc_m(x,r)}{dr}. \tag{60}$$

We assume that the diffusion is effective enough that dc_m/dx can be regarded as independent of r, so that this equation can easily be integrated when Eq. (59) is substituted for $\dot{m}_{2,s}(r)$. The result is

$$c_m(x,r)=E+\frac{dc_m}{dx}\left[x+\frac{\dot{m}_{2,s,w}}{\rho_m D}\left(\frac{r^4}{8R^2}-\frac{r^2}{4}\right)\right], \tag{61}$$

with E an r-independent constant of integration that we have no need to evaluate. Then, the mixing flux can easily be obtained by integrating the product of Eqs. (59) and (61)

$$\dot{N}_{H,4,\mathrm{stream}}=\frac{1}{m_H}\int_0^R c_m\dot{m}_{2,s}\,2\pi r\,dr \tag{62}$$

$$=-\frac{\pi}{48}\frac{dc_m}{dx}\frac{\dot{m}_{2,s,w}^2R^4}{m_H\rho D} \tag{63}$$

$$\sim-\frac{\pi}{48}\frac{dn_H}{dx}\frac{m_L}{m_{\mathrm{avg}}^2}\frac{|p_1|^2|\langle u_1\rangle|^2R^4}{a^4\rho D}, \tag{64}$$

where the r-independent terms in Eq. (61) disappear in the integration, and the final step simply requires substitution of Eqs. (2) and (58).

To judge the seriousness of the threat imposed by this fourth-order effect, we can take the ratio of $\dot{N}_{H,4,\mathrm{stream}}$ to the intrinsic remixing described by the $|U_1|^2$ term at the end of Eq. (56). Using the simple identities $\rho_m a^2=\gamma p_m$ and $A=\pi R^2$, we obtain

$$\frac{\dot{N}_{H,4,\mathrm{stream}}}{\dot{N}_{\mathrm{intrinsic}}}\sim\frac{1}{12}\frac{m_L}{m_{\mathrm{avg}}}\frac{R^3}{F_{\mathrm{grad}}\delta_\kappa\delta_D^2}\frac{|p_1|^2}{\gamma^2p_m^2}. \tag{65}$$

With F_{grad} and m_L/m_{avg} of order unity and, typically, $|p_1|/p_m$ no larger than approximately 0.1, we see that it is probably necessary to keep R less than 10 δ if we want to keep the mixing effect of streaming acceptably small. For the experiments described below, we always have $R\leqslant 4.8\,\delta_\kappa$ and $R\leqslant 4.5\,\delta_D$, and $|p_1|/p_m\leqslant 0.03$, so we anticipate no significant contribution from streaming. However, we must keep in mind the approximate nature of Eq. (58). This is only a rough estimate, and other circumstances can easily violate the approximations leading to Eq. (65).

VII. COMPARISON WITH EXPERIMENT

The mole flux expanded to second order in the acoustic variables is seen from Eqs. (41), (44), and (56) to be linear in the concentration gradient dn_H/dx. The contribution from streaming is also proportional to dn_H/dx, but it was estimated above to be too small to detect under our experimental conditions. Considering terms through second order, then, we can calculate the saturation gradient easily by setting $\dot{N}_H=0$. For example, if the duct is so narrow that ordinary diffusion can be neglected, one finds from Eq. (56) that the final separation in the boundary-layer limit is a sinusoidal function of the phasing

$$\frac{dn_H}{dx}=-\frac{\gamma-1}{\gamma}\frac{\omega k_T A}{p_m}\frac{|p_1|}{|U_1|}\frac{F_{\mathrm{trav}}\cos\theta+F_{\mathrm{stand}}\sin\theta}{F_{\mathrm{grad}}}. \tag{66}$$

Although the boundary-layer approximation yields the most compact expression for the separation flux, the expression remains qualitatively the same regardless of the duct geometry. We have therefore used our circular-tube calculation from Sec. V to calculate the expected final separations corresponding to the two tubes studied in our experiment. The narrower of the two tubes described below was chosen so that $\dot{N}_{H,m}$ and $\dot{N}_{H,4,\mathrm{stream}}$ would be small and the new term from Sec. V proportional to $|U_1|^2$ would be emphasized. The wider tube, in contrast, was selected in order to demonstrate the convergence of the exact, circular-tube calculation to that of the boundary-layer limit derived in Sec. V.

In order to test our theory experimentally, we used the apparatus presented in Ref. 2. The acoustic field inside the tube was provided by the compressions of metal bellows housed in closed reservoirs at either end. The bellows were driven by independent linear motors, so that we could create arbitrary phasings and amplitudes in the sound field. Two ducts were studied, the first of which was a copper tube 4.75 mm in diameter and $l=0.914$ m long, driven at 10 Hz with pressure amplitudes as high as 2.5 kPa. The second, wider duct was a stainless-steel tube of 1.52 cm diameter and 0.912 m length, driven at 15 Hz at amplitudes up to 1.25 kPa. The sample was a 50–50 mixture of helium and argon at room

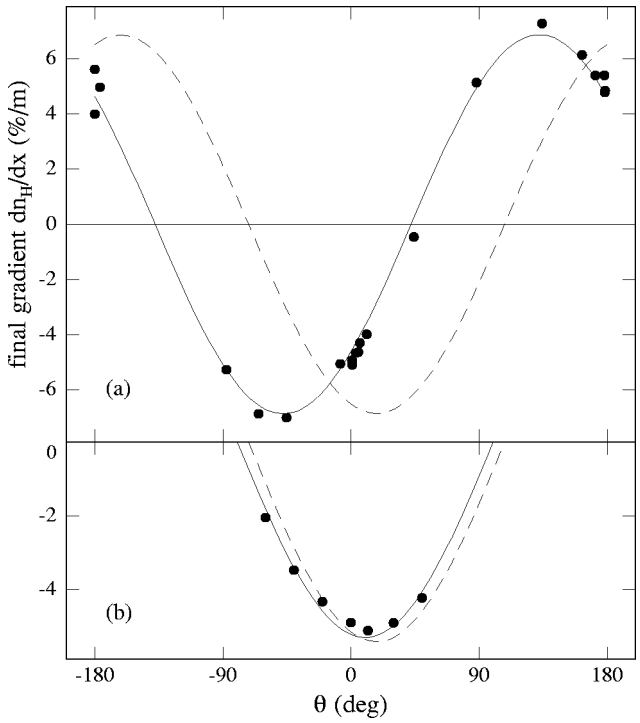

FIG. 5. Dependence of final separation on the phasing between p_1 and U_1. (a) Data for the 4.75-mm tube are scaled to $|Z|=70$ MPa·s/m^3. The solid curve is generated from an exact calculation for this circular tube and includes the effect of steady diffusion from Eq. (44). The dashed curve is the boundary-layer limit calculation for the narrow tube and also includes the remixing from steady diffusion. The boundary-layer expression is inappropriate for the 4.75-mm tube, because the radius of the tube is not much greater than the boundary-layer thickness. Although the boundary-layer calculation deviates greatly from the exact calculation and from the data in its periodic phase dependence, it still yields a reasonable value for the magnitude of the maximum separation. (b) For the 1.52-cm tube, all data were taken with $|Z|=10$ MPa·s/m^3 and $|p_1||U_1|=0.1$ W. The solid curve is again the result of a circular-tube calculation, while the dashed curve is the boundary-layer limit calculation. For the 1.52-cm tube, $R\sim 5\,\delta$ and the boundary-layer calculation is fairly accurate.

temperature and at a mean pressure of 80 kPa, which is approximately the local atmospheric pressure. Complex pressure amplitudes $p_{1,\mathrm{top}}$ and $p_{1,\mathrm{bottom}}$ were measured in the two reservoirs using piezoresistive transducers and lock-in amplifiers. From these measurements we inferred the wave in the tube to be

$$p_1(x)=p_{1,\mathrm{bottom}}\frac{\sin k(l-x)}{\sin kl}+p_{1,\mathrm{top}}\frac{\sin kx}{\sin kl}, \tag{67}$$

and

$$U_1(x)=\frac{\imath(1-f_\nu)A}{\omega\rho_m}\frac{dp_1}{dx}, \tag{68}$$

where $x=0$ at the bottom end of the tube and the complex wave number is given by

$$k=\frac{\omega}{a}\sqrt{\frac{1+(\gamma-1)f_\kappa}{1-f_\nu}}. \tag{69}$$

We evaluate a, ρ_m, f_ν, and f_κ using properties of the 50–50 mixture (ignoring their x dependence for $dc_m/dx\neq 0$), and we use the Bessel-function expressions for f_ν and f_κ. For the display of data here, we use p_1 and U_1 at $x=l/2$.

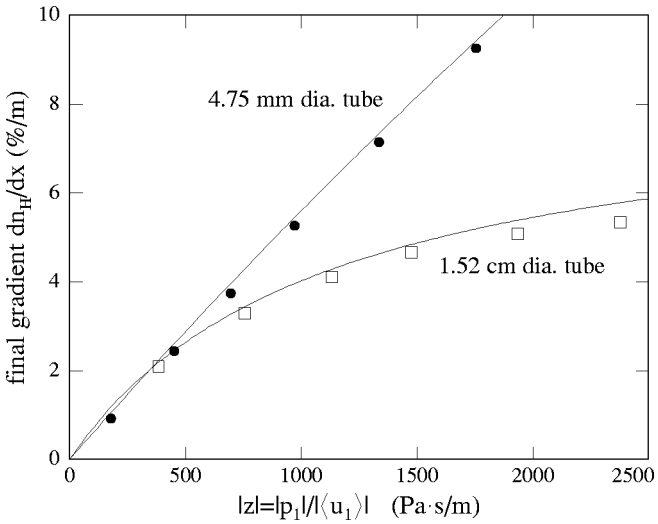

FIG. 6. The saturation value of the concentration gradient as a function of specific acoustic impedance $|z|$ for fixed $|p_1||U_1|$ and fixed phasing θ. For the 4.75-mm tube, $|p_1||U_1|=0.05$ W and $\theta=-45°$, while for the 1.52-cm tube $|p_1||U_1|=0.1$ W and $\theta=12°$. Points are measurements, and lines are circular-tube calculations.

The first verification of our circular-tube calculation for an arbitrary-diameter tube was in experimentally demonstrating the calculated dependence on phase θ for the narrow cylindrical tube. The data are compared against our theory, both in the boundary-layer limit and in the exact case for our geometry, in Fig. 5(a). Not all the data for the 4.75-mm tube in this figure were taken at the exact same value of $|p_1||U_1|$ or of acoustic impedance $Z=p_1/U_1$. Because the values of $|Z|$ varied over an order of magnitude among the data, the fractional separation for each point was normalized to an intermediate value of $|Z|$ by multiplying by (70 MPa $\cdot$s/m^3)/$|Z|$, as suggested by Eq. (66). This scaling is valid if $\dot{N}_{H,m}$ and $\dot{N}_{H,4,\mathrm{stream}}$ are much smaller than $\dot{N}_{H,2}$. Neverthe-

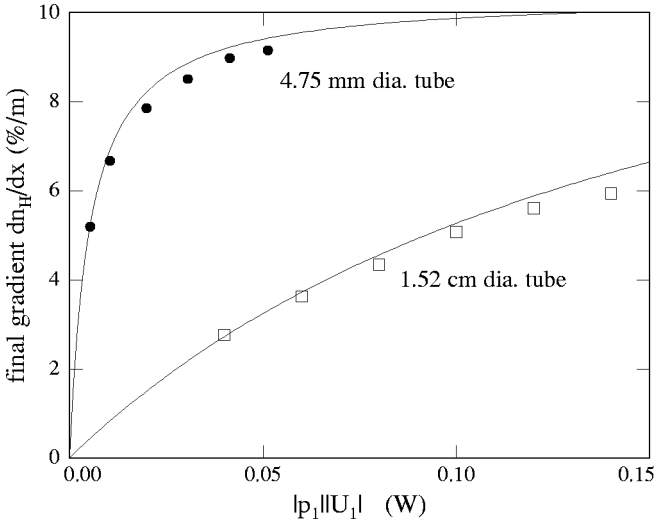

FIG. 7. The saturation gradient with varying $|p_1||U_1|$ and with $|Z|$ now held fixed. For the narrow tube, $|Z|=100$ MPa·s/m^3 and $\theta=-45°$, and for the wide tube, $|Z|=10$ MPa·s/m^3 and $\theta=12°$. Points are measurements, and lines are circular-tube calculations. In the absence of ordinary diffusion or acoustic streaming, each curve would be a horizontal line with dn_H/dx at its asymptotic value for $|p_1||U_1|\to\infty$.

less, there are small ($\sim$15%) deviations in $|p_1||U_1|$ between the points, which cause some of the scatter in the data through the presence of the $\dot{N}_{H,m}$ term. Several data points are also shown in Fig. 5(b) for the phase dependence of separation in the 1.52-cm tube. In this case, the boundary-layer and circular-tube calculations give quite similar results, although the circular-tube calculation is still in better agreement with the data.

In view of Eqs. (41), (44), and (56), one is able to demonstrate the effect of each remixing term by varying $|p_1||U_1|$ and $|Z|$ independently, while maintaining a fixed phasing of the acoustic field in the tube. In order to minimize errors arising from small deviations in the experimental phasing, and to maximize the resolution of our separation measurement, we chose that value of θ that yielded the greatest final separation for each tube. As seen in Fig. 5, for the narrow tube this angle was approximately $-45°$, whereas for the wide tube the maximum was at 12°; the boundary-layer calculation gives the largest gradient at saturation for $\theta \sim 18°$. Figure 6 shows the nearly linear relationship between final gradient and specific acoustic impedance for the narrow tube, which is in very good agreement with our calculations. The deviation of the filled circles and their associated curve from a linear relationship is almost entirely due to the flux from ordinary diffusion, $\dot{N}_{H,m}$: had we held $|U_1|^2$ constant instead of $|p_1||U_1|$, the function would be a straight line.

The small deviations of the data from the calculated curves may derive from several sources. First, the saturation gradient $(dn_H/dx)_{\text{sat}}$ depends on n_H, which itself varies along the length of the tube. We have not calculated the exact profile of n_H along the tube, although one can in principle do so for our apparatus using the fact that the system is closed so that the total number of moles of each gas is conserved. Second, the thermophysical properties of the gas mixture are calculated as in Giacobbe[12] and may contain errors of a few percent at our operating pressure and temperature for the 50–50 mixture. Finally, no effort was made to accurately control the temperature of the apparatus, and the ambient temperature of the laboratory varied by as much as 5 °C over the course of an experiment.

Data for the wide tube are also shown in Fig. 6. The nonlinearity of the saturation gradient vs specific acoustic impedance is much more pronounced in this case than for the narrow tube. Although $|p_1||U_1|$ for these data is twice that of the narrow-tube data, the area of the wide tube is ten times greater, so that the remixing flux from steady diffusion is proportionately higher.

In Fig. 7, we show the effect of the diffusion term more clearly by varying $|p_1||U_1|$ at constant $|Z|$. Steady diffusion competes more effectively with the separation process when the separation rate is made small. In view of Eq. (64), the saturation gradient should begin to decrease again at higher values of $|p_1||U_1|$ due to streaming. However, we are not able to attain such large values of $|p_1||U_1|$ in our apparatus, and other nonlinear effects may set in that limit the applicability of our analysis for such operating conditions.

ACKNOWLEDGMENTS

This work was supported by the Office of Basic Energy Sciences in the U.S. Department of Energy under contract No. W-7405-ENG-36. The authors are grateful to Phil Spoor and Scott Backhaus for several useful discussions.

[1] G. W. Swift, and P. S. Spoor, "Thermal diffusion and mixture separation in the acoustic boundary layer," J. Acoust. Soc. Am. **106**, 1794 (1999); **107**, 2299(E) (2000); **109**, 1261(E) (2001).

[2] P. S. Spoor and G. W. Swift, "Thermoacoustic separation of a He–Ar mixture," Phys. Rev. Lett. **85**, 1646 (2000).

[3] Thermal diffusion was first discovered theoretically from the kinetic theory of gases by D. Enskog and S. Chapman independently. An account including the original references can be found in K. E. Grew and T. L. Ibbs, *Thermal Diffusion in Gases* (Cambridge University Press, Cambridge, 1952).

[4] B. E. Atkins, R. E. Bastick, and T. L. Ibbs, "Thermal diffusion in mixtures of inert gases," Proc. R. Soc. London, Ser. A **172**, 142–158 (1939).

[5] L. D. Landau and E. M. Lifshitz, *Fluid Mechanics* (Pergamon, New York, 1982).

[6] The hydraulic radius r_h of a tube or duct is defined as the ratio of its cross section to its perimeter. For a right circular cylinder, the hydraulic radius is equal to one half of the cylinder radius.

[7] Readers who are familiar with standing-wave thermoacoustic engines and refrigerators will recognize that the above discussion is similar to the description of the critical temperature gradient, which differs from $(dc_m/dx)_{\text{sat}}$ by the factor k_T'/T_m.

[8] Note that Eqs. (15) and (16) may equally well be expressed in terms of the mole fraction. Use of Eqs. (2) and (5) shows that these are equivalent to

$$\left(\frac{dn_H}{dx}\right)_{\text{sat}} = \frac{\gamma-1}{\gamma} k_T \frac{|p_1|}{p_m} \frac{\omega}{|\langle u_1 \rangle|}, \quad \text{and} \quad \Gamma_c = \frac{dn_H/dx}{(dn_H/dx)_{\text{sat}}}.$$

[9] For consistency with the prior literature, we denote the longitudinal direction along the tube by x. Where we refer to cylindrical coordinates, then, we consider the set to be (x,r,ϕ).

[10] E. J. Watson, "Diffusion in oscillating pipe flow," J. Fluid Mech. **133**, 233–244 (1983).

[11] W. L. M. Nyborg, "Acoustic Streaming," in *Physical Acoustics*, edited by W. P. Mason (Academic, New York, 1965), Vol. II B, pp. 265–331.

[12] F. W. Giacobbe, "Estimation of Prandtl numbers in binary mixtures of helium and other noble gases," J. Acoust. Soc. Am. **96**, 3568–3580 (1994).